EUROPHYSICS LETTERS 15 September 2000

Europhys. Lett., **51** (6), pp. 641–647 (2000)

Breakdown of Pippard ineffectiveness condition for phonon-electron scattering in micro and nanostructures

A. Sergeev and V. Mitin

Department of ECE, Wayne State University - Detroit, MI 48202, USA

(received 6 December 1999; accepted in final form 20 July 2000)

PACS. 63.20.Kr – Phonon-electron and phonon-phonon interactions.
PACS. 72.10.-d – Theory of electronic transport, scattering mechanisms.

Abstract. – The Pippard ineffectiveness condition —that electrons strongly scattering from impurities and defects are ineffective in scattering phonons— is based on the assumption that electron scatterers vibrate in the same way as the host lattice. Then the relaxation rate of a low-energy phonon with the wave vector q is $1/\tau_{\text{ph-e}} \sim u^2 q^2 l/v_{\text{F}}$ (u and v_{F} are the sound velocity and Fermi velocity, l is the electron mean free path). Boundaries and defects moving differently from host lattice drastically change the character of the interference between scattering processes and increase the phonon-electron coupling. In the presence of the quasistatic potential the phonon relaxation is $(q^2 lL)^{-1}$ times faster: $1/\tau_{\text{ph-e}} \sim u^2/(v_{\text{F}} L)$ (L is the electron mean free path with respect to scattering from the quasistatic potential). Analogous effect is expected for phonons with $\omega \sim 0.01\omega_{\text{D}}$ (ω_{D} is the Debye frequency) in conductors with substitutional disorder.

In many cases the interference between different scattering mechanisms significantly modifies their total effect. More than six decades ago such problems were discussed by Peierls [1], who studied the interaction between the long-wave phonons and other phonons with short mean free path. Extending this work, Pippard [2] has considered the interaction between phonons and electrons scattering from impurities and defects. According to ref. [2], the phonon-electron interaction depends essentially on the parameter ql, where q is the wave vector of a phonon, and l is the electron mean free path. In the hydrodynamic limit, $ql < 1$, the phonon-electron coupling is a factor of ql weaker than the coupling in the pure limit, $l \to \infty$. This statement is well known as the Pippard ineffectiveness condition [3, 4]. It was employed in many areas of metal and semiconductor physics [3–5]. Pippard's results were confirmed by microscopic calculations by Grünvald and Sharnberg [6].

Pippard's consideration is based on the assumption that due to scattering from impurities electrons relax to the equilibrium distribution in the local coordinate system moving with the local lattice. The local lattice velocity plays a role of the hydrodynamical variable. Such treatment assumes that electrons are dragged by scatterers (impurities and defects), which in turn are completely dragged by the host lattice. Obviously this assumption is not valid in the presence of rigid boundaries or defects with mass significantly different from mass of the host atom.

In the current paper we calculate the relaxation rate of longitudinal and transverse phonons in metallic stuctures, where electrons scatter from impurities dragged by the lattice and also from the quasistatic potential. We also evaluate the effect of substitutional disorder on phonon-electron coupling.

Following Grünvald and Sharnberg [6], we consider the Hamiltonian, which describes the "pure" electron-phonon interaction and the interaction between electrons and impurities that are completely dragged by lattice [7],

$$H_{\rm int} = \sum_{\boldsymbol{p},\boldsymbol{q}} g(\boldsymbol{q}) c^{\dagger}_{\boldsymbol{p}+\boldsymbol{q}} c_{\boldsymbol{p}} (b_{\boldsymbol{q},n} + b^{\dagger}_{-\boldsymbol{q},n}) + \sum_{\boldsymbol{p},\boldsymbol{k},\boldsymbol{R}_\alpha} V_{\text{e-imp}}(\boldsymbol{k}) c^{\dagger}_{\boldsymbol{p}} c_{\boldsymbol{p}-\boldsymbol{k}} \exp[-i\boldsymbol{k}\boldsymbol{R}_\alpha] + \\ + \sum_{\boldsymbol{p},\boldsymbol{k},\boldsymbol{q},\boldsymbol{R}_\alpha} \gamma(\boldsymbol{k},\boldsymbol{q}) c^{\dagger}_{\boldsymbol{p}} c_{\boldsymbol{p}-\boldsymbol{k}} (b_{\boldsymbol{q},n} + b^{\dagger}_{-\boldsymbol{q},n}) \exp[-i(\boldsymbol{k}-\boldsymbol{q})\boldsymbol{R}_\alpha], \tag{1}$$

where $c^{\dagger}_{\boldsymbol{p}}$ is the electron creation operator, $b^{\dagger}_{\boldsymbol{q},n}$ is the creation operator of a phonon with a wave vector $\boldsymbol{q}$ and polarization index n, and $\boldsymbol{R}_\alpha$ are the equilibrium positions of impurities.

The vertex of pure phonon-electron scattering is given by

$$g = (2\epsilon_{\rm F}/3)\ ((\boldsymbol{q}\cdot\boldsymbol{e}_n)/(2\rho\omega)^{1/2})\,, \tag{2}$$

where $\epsilon_{\rm F}$ is the Fermi energy, $\boldsymbol{e}_n$ is the phonon polarization vector, ρ is the density.

The second term describes elastic electron-impurity scattering. The screened electron-impurity potential is

$$V_{\text{e-imp}} = -4\pi(Z_{\rm imp} - Z_{\rm ion})/\kappa^2, \qquad \kappa^2 = 4\pi e^2\nu, \qquad \nu = m p_{\rm F}/\pi^2. \tag{3}$$

The vertex of inelastic electron-impurity scattering is given by [6, 8]

$$\gamma(\boldsymbol{k},\boldsymbol{q}) = -iV_{\text{e-imp}}(\boldsymbol{k}\boldsymbol{e}_n)/(2\rho\omega_q)^{1/2}\,. \tag{4}$$

The inelastic electron-impurity scattering is characterized by a large value of the electron momentum transferred to impurity ($k \sim p_{\rm F}$), while the transferred energy is the same as in the pure phonon-electron interaction.

The electrical resistivity determined by the Hamiltonian in the form of eq. (1) is

$$\rho(T) = \rho_0 + \rho_{\rm BG}(T) + \rho_{\rm int}(T), \tag{5}$$

where ρ_0 is the residual resistivity due to elastic electron-impurity scattering, $\rho_{\rm BG}$ is the Bloch-Grüneisen term due to the pure electron-phonon scattering. The interference term, $\rho_{\rm int}$, is determined by the inelastic electron-impurity scattering and quantum nonequlibrium corrections to the processes of pure electron-phonon scattering [8]. If $T > u/l$, the interference term has the form $\rho_{\rm int} = B\rho_0 T^2$, the longitudinal phonons give a negative correction to the resistivity, while the transverse phonons result in a positive correction [8, 9].

Now we modify the Grünvald and Sharnberg model. We suggest that the elastic electron scattering is not only due to the potential that moves together with vibrating atoms of the host lattice. We accept that the electron lifetime in the electron Green function is shorter than the momentum relaxation time due to vibrating scattering potential. We will show that any additional electron damping destroys interference compensation of strong scattering processes and results in an enhancement of the phonon-electron interaction due to disorder. In our opinion, this model is relevant to the electron scattering from rigid boundaries of micro and nanostructures. It also allows one to evaluate the effect of substitutional disorder on phonon-electron coupling.

We present the total momentum relaxation rate $(1/\tau)$ in the form

$$\tau^{-1} = \tilde{\tau}^{-1} + \tau_{\rm qs}^{-1}, \tag{6}$$

where $1/\tilde{\tau}$ is the electron momentum relaxation rate due to scattering from vibrating impurities, and $1/\tau_{\rm qs}$ is the relaxation rate due to the additional quasistatic potential. Therefore, in our case the residual resistivity is $\rho_0 = 3/(e^2\nu v_{\rm F}^2\tau)$.

Note that the vertex of inelastic electron-impurity scattering also consists of the impurity potential, which may be expressed through the corresponding momentum relaxation rate,

$$N_{\rm imp} V^2_{\text{e-imp}} = (\pi\nu\tilde{\tau})^{-1}, \tag{7}$$

where $N_{\rm imp}$ is the concentration of impurities.

Electron retarded (advanced) Green function taking into account the elastic electron scattering from impurities and boundaries is given by

$$G_0^{\rm R}(\boldsymbol{p},\epsilon) = [G_0^{\rm A}(\boldsymbol{p},\epsilon)]^* = (\epsilon - \xi_p + i/2\tau)^{-1}, \tag{8}$$

where $\xi_p = (p^2 - p_{\rm F}^2)/2m$. Here we introduce the following notations for integrals of electrons Green functions:

$$\zeta_n = \frac{1}{\pi\nu\tau}\int \frac{{\rm d}\boldsymbol{p}}{(2\pi)^3} G^{\rm A}(\boldsymbol{p},\epsilon) G^{\rm R}(\boldsymbol{p}+\boldsymbol{q},\epsilon+\omega) y^n, \tag{9}$$

where $y = (\boldsymbol{p}\cdot\boldsymbol{q})/(pq)$. If $\omega\tau \ll (ql)^2$,

$$\zeta_0 = \arctan(ql)/(ql), \qquad i\zeta_1 = (1-\zeta_0)/(ql), \qquad \zeta_2 = (1-\zeta_0)/(ql)^2.$$

In the model under consideration, phonons scatter only from electrons due to the pure electron-phonon interaction and also by means of vibrating impurities. These processes will be taken into account in the first order of perturbation theory. Thus, we may ignore phonon damping in the phonon Green function,

$$D^{\rm R}(\boldsymbol{q},\omega) = (\omega - \omega_{\boldsymbol{q}} + i0)^{-1} + (\omega + \omega_{\boldsymbol{q}} + i0)^{-1}. \tag{10}$$

Employing the Keldysh diagrammatic technique, we describe the electron and phonon systems by the matrix Green functions with retarded ($G^{\rm R} = G_{21}$), advanced ($G^{\rm A} = G_{12}$) and kinetic ($G^{\rm C} = G_{22}$) components. The kinetic components may be presented as

$$G^{\rm C}(\boldsymbol{p},\epsilon) = (2n_\epsilon + 1)2i{\rm Im}G^{\rm A}(\boldsymbol{p},\epsilon), \qquad D^{\rm C}(\boldsymbol{q},\omega) = (2N_\omega + 1)2i{\rm Im}D^{\rm R}(\boldsymbol{q},\omega), \tag{11}$$

where n_ϵ and N_ω are the electron and phonon distribution functions.

In the Keldysh technique, vertices are multiplied by the tensor K_{ij}^k ($K_{ij}^1 = \delta_{ij}/\sqrt{2}$, and $K_{ij}^2 = (\sigma_x)_{ij}/\sqrt{2}$) with an upper phonon index and lower electron indices. In what follows, we will present only vertex components with phonon index $k = 2$. In the canonical collision integral, these components give a term, which is proportional to $(2N_\omega + 1)(n_{\epsilon+\omega} - n_\epsilon)$.

Following refs. [6,8,10], we build effective vertices Γ and Λ, shown in fig. 1. The vertex Γ, taking into account elastic and inelastic electron-impurity scattering, is

$$\Gamma_{11}^2 = \frac{\boldsymbol{p}\cdot\boldsymbol{e}_n}{\tilde{\tau}(\rho\omega)^{1/2}}(n_\epsilon - n_{\epsilon+\omega}), \tag{12}$$

for $k = 2$ all other components are zero.

The vertices Γ_{ij}^k and g_{ij}^k are strongly renormalized due to elastic electron scattering. As a result, we obtain the vertex Λ_{ij}^k shown in fig. 1,

$$\Lambda_{11}^2 = \frac{2ig}{\sqrt{2}}\left(\frac{\zeta_0^*}{1-\zeta_0^*} - \frac{3}{(ql)^2}\frac{\tau}{\tilde{\tau}}\right)(n_\epsilon - n_{\epsilon+\omega}). \tag{13}$$

The kinetic equation for the phonon distribution function $N(\omega_q)$ has the form

$$\frac{{\rm d}N(\omega_q)}{{\rm d}t} = -i\int \frac{{\rm d}\omega}{(2\pi)}{\rm Im}D^{\rm R}(\boldsymbol{q},\omega)\ [2i(2N_\omega+1){\rm Im}\Pi^{\rm R}(\boldsymbol{q},\omega) - \Pi^{\rm C}(\boldsymbol{q},\omega)], \tag{14}$$

where the right-hand side of the last equation is the collision integral $I(\omega_q)$ expressed through the phonon self-energy, $\Pi^{\rm A(C)}$ is the advanced (kinetic) phonon-electron self-energy. All possible phonon self-energy diagrams with vertices γ, Γ, g, Λ are presented in fig. 2.

Let us first consider longitudinal phonons. The collision integral based on the first diagram is given by

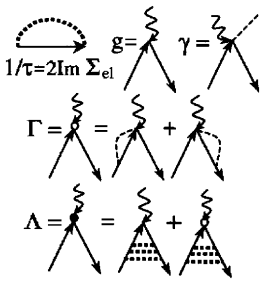

Fig. 1

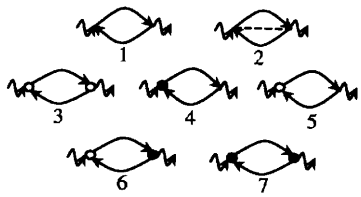

Fig. 2

Fig. 1 – Electron self-energy due to elastic scattering (the thick dashed line presents the total potential) and vertices of the phonon-electron interaction γ, Γ, g and Λ.

Fig. 2 – Phonon self-energy diagrams.

$$I_1(\omega_q) = \int \frac{\mathrm{d}\epsilon}{2\pi}\frac{\mathrm{d}\omega}{2\pi}\frac{\mathrm{d}\boldsymbol{p}}{(2\pi)^3} g^2 \mathrm{Re}G^{\mathrm{R}}(\boldsymbol{p},\epsilon) G^{\mathrm{A}}(\boldsymbol{p}+\boldsymbol{q},\epsilon+\omega)\mathrm{Im}D^{\mathrm{R}}(\boldsymbol{q},\omega) R(\epsilon,\omega), \tag{15}$$

where

$$R(\epsilon,\omega) = N_\omega n_\epsilon (1-n_{\epsilon+\omega}) - (1+N_\omega)(1-n_\epsilon) n_{\epsilon+\omega}. \tag{16}$$

Integrating, we present I_1 in the form

$$I_1(\omega_q) = -2\beta_{\mathrm{l}}\omega_q \tau \int \mathrm{d}\epsilon R(\epsilon,\omega_q)\mathrm{Re}F_1(q), \qquad F_1(q) = \zeta_0(q), \tag{17}$$

where the dimensionless coupling constant is given by $\beta_{\mathrm{l}} = (2\epsilon_{\mathrm{F}}/3)^2\nu/2\rho u_{\mathrm{l}}^2$, and u_{l} is the longitudinal sound velocity.

Calculations show that contributions of all other diagrams may be presented in the form of eq. (17) with the following functions:

$$\begin{aligned} F_2 &= \frac{\tau}{\tilde\tau}\frac{3}{(ql)^2}, \qquad F_3 = -\left(\frac{\tau}{\tilde\tau}\right)^2 \frac{9}{(ql)^2}\zeta_2, \qquad F_4 = -\frac{\tau}{\tilde\tau}\frac{6i}{ql}\zeta_1, \\ F_5 &= \left(\frac{\zeta_0}{1-\zeta_0} - \frac{\tau}{\tilde\tau}\frac{3}{(ql)^2}\right)\zeta_0, \qquad F_6 = -3i\frac{\tau}{\tilde\tau}\left(\frac{\zeta_0}{1-\zeta_0} - \frac{\tau}{\tilde\tau}\frac{3}{(ql)^2}\right)\zeta_1, \qquad F_7 = 0. \end{aligned} \tag{18}$$

Substituting the functions F_i into eq. (17) and summing the contributions of all diagrams, we obtain the collision integral, which describes the interaction between longitudinal phonons and electrons in a disordered conductor,

$$I_{\mathrm{l.ph\text{-}e}} = -2\beta_{\mathrm{l}}\frac{u_{\mathrm{l}}}{v_{\mathrm{F}}}\int \mathrm{d}\epsilon R(\epsilon,\omega_q)\left(\frac{ql\zeta_0}{1-\zeta_0} - \frac{\tau}{\tilde\tau}\frac{3}{(ql)^2}\right). \tag{19}$$

The phonon relaxation rate is determined as

$$\frac{1}{\tau_{\mathrm{ph\text{-}e}}(\epsilon)} = -\frac{\delta I_{\mathrm{ph\text{-}e}}}{\delta N_\omega}(N_\omega = N_\omega^{\mathrm{equ}}, n_\epsilon = n_\epsilon^{\mathrm{equ}}), \tag{20}$$

where N_ω^{equ} and $n_\epsilon^{\mathrm{equ}}$ are equilibrium distribution functions. Using eq. (19), we find

$$\frac{1}{\tau_{\mathrm{l.ph\text{-}e}}} = 2\beta_{\mathrm{l}}\omega_q\frac{u_{\mathrm{l}}}{v_{\mathrm{F}}}\left[\frac{ql\arctan ql}{ql-\arctan ql} - \frac{\tau}{\tilde\tau}\frac{3}{ql}\right]. \tag{21}$$

Only the second and third diagrams give a contribution to the relaxation of transverse phonons. The corresponding collision integral is

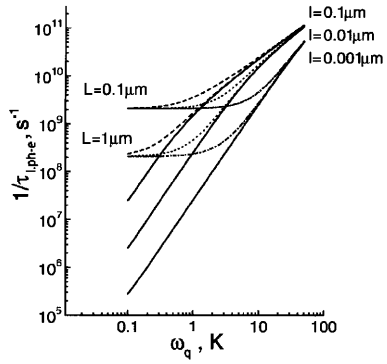

Fig. 3

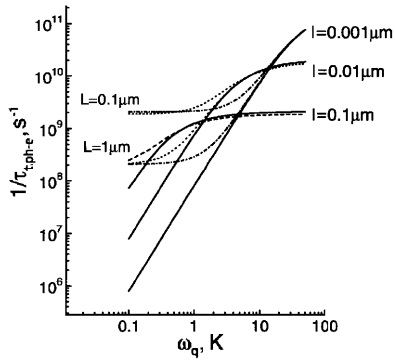

Fig. 4

Fig. 3 – Relaxation rate of longitudinal phonons in Al structures. Solid curves correspond to complete drag of scatterers, $L = \infty$. Dashed ($l = 0.1\,\mu$m), dotted ($l = 0.01\,\mu$m) and dash-dotted ($l = 0.001\,\mu$m) curves: the electron mean free paths with respect to scattering from the quasistatic potential L are $0.1\,\mu$m and $1\,\mu$m.

Fig. 4 – Relaxation rate of transverse phonons in Al structures. Solid curves: $L = \infty$. Dashed ($l = 0.1\,\mu$m), dotted ($l = 0.01\,\mu$m) and dash-dotted ($l = 0.001\,\mu$m) curves: $L = 0.1\,\mu$m and $1\,\mu$m.

$$I_{\text{t.ph-e}} = -2\beta_{\text{t}}\frac{u_{\text{t}}}{v_{\text{F}}}\frac{\tau}{\tilde{\tau}}\int \mathrm{d}\epsilon R(\epsilon,\omega_q)\frac{3}{ql}\left[1-\frac{3}{2}\frac{\tau}{\tilde{\tau}}(\zeta_0-\zeta_2)\right], \tag{22}$$

where $\beta_{\text{t}} = (2\epsilon_{\text{F}}/3)^2\nu/2\rho u_{\text{t}}^2$, and u_{t} is the transverse sound velocity.

The relaxation rate of a transverse phonon is

$$\frac{1}{\tau_{t.ph-e}} = \frac{6\beta_{\text{t}}u_{\text{t}}^2}{v_{\text{F}}l}\,\frac{\tau}{\tilde{\tau}}\left(1+\frac{\tau}{\tilde{\tau}}\,\frac{3ql-3(ql)^2\arctan(ql)-3\arctan(ql)}{2(ql)^3}\right). \tag{23}$$

Note, that the factor $(1-\tau/\tilde{\tau})$ may be expressed as l/L, where L is the electron mean free path with respect to the scattering from the quasistatic potential. Then, in the impure limit $ql < 1$, the phonon relaxation rate may be presented as

$$\frac{1}{\tau_{\text{l.ph-e}}} = \frac{6\beta_{\text{l}}u_{\text{l}}^2}{v_{\text{F}}L} + \frac{8}{5}\beta_{\text{l}}\tau\omega_q^2, \tag{24}$$

$$\frac{1}{\tau_{\text{t.ph-e}}} = \frac{6\beta_{\text{t}}u_{\text{t}}^2}{v_{\text{F}}L}\left(1-\frac{l}{L}\right) + \frac{6}{5}\beta_{\text{t}}\tau\omega_q^2\left(1-\frac{l}{L}\right). \tag{25}$$

The second term in eq. (24) and in eq. (25) represents the Pippard result: the relaxation rate is ql times slower than the relaxation rate of longitudinal phonons in a pure conductor. The first terms describe a new effect: due to scattering from quasistatic potential, the phonon relaxation rate enhances by a factor $\sim 1/(q^2lL)$ when compared to the Pippard result.

To illustrate our results, we calculate the phonon-electron relaxation rate in Al structures. We use the following parameters of Al [8]: $u_{\text{l}} = 6.3\cdot 10^5$ cm/s, $u_{\text{t}} = 3.1\cdot 10^5$ cm/s, $v_{\text{F}} = 13\cdot 10^7$ cm/s, $\beta_{\text{l}} = 1.14$, and $\beta_{\text{t}} = 4.7$. Temperature dependencies of the phonon-electron relaxation rate are presented in figs. 3 and 4. Solid curves correspond to the Pippard case of complete drag of electron scatterers by phonons. The relaxation rate of longitudinal and transverse low-energy phonons is proportional to $\omega_q^2 l$. The relaxation rate of high-energy longitudinal phonons is proportional to $\omega_q l^0$, the corresponding relaxation rate of transverse phonons is independent of ω_q and proportional to l^{-1}. The dashed, dotted and dashed-dotted curves present the phonon relaxation rate in structures with quasistatic electron scattering

potential of rigid boundaries and heavy defects. The electron mean free path with respect to the quasistatic potential, L, is taken to be $0.1\,\mu$m and $1\,\mu$m. The phonon relaxation rate depends on both parameters, l and L. As is seen from figs. 3 and 4, even if the electron mean free path with respect to the total scattering potential, l, is significantly shorter than L, the relaxation rate of low-energy phonons changes drastically. As we have already mentioned, the asymptotic value of the relaxation rate turns out to be $\sim u^2/v_{\mathrm{F}}L$.

Finally, we calculate the heat flux from hot electrons with the temperature θ to phonons with the temperature T. It is expressed in terms of the phonon-electron collision integral,

$$Q = \int \frac{\mathrm{d}\boldsymbol{q}}{(2\pi)^3}\ \omega_q I_{\text{ph-e}}(\theta, T). \tag{26}$$

Using eqs. (19) and (22), we obtain that at low temperatures, $\theta < u/l$, the heat flux is

$$\begin{aligned} Q \;=\; & \frac{\pi^4\nu}{5p_{\mathrm{F}}L}\left[\frac{\beta_{\mathrm{l}}}{p_{\mathrm{F}}u_{\mathrm{l}}} + \frac{2\beta_{\mathrm{t}}}{p_{\mathrm{F}}u_{\mathrm{t}}}\left(1-\frac{l}{L}\right)\right](\theta^4 - T^4) + \frac{96\pi^6\nu}{925}(p_{\mathrm{F}}l)\times \\ & \times\left[\frac{\beta_{\mathrm{l}}}{(p_{\mathrm{F}}u_{\mathrm{l}})^3} + \frac{3\beta_{\mathrm{t}}}{2(p_{\mathrm{F}}u_{\mathrm{t}})^3}\left(1-\frac{l}{L}\right)\right](\theta^6 - T^6), \end{aligned} \tag{27}$$

where the first term describes the increase of the phonon-electron coupling due to static disorder, and the second term corresponds to the Pippard ineffectiveness condition [10, 11]. Note that in the pure conductor the heat flux is proportional to $\theta^5 - T^5$ [12]. Thus, the second term is approximately $(\theta l/u)^{-1}$ times smaller, while the first term is $(\theta L/u)^{-1}$ times larger than the heat flux in a pure conductor [12].

Possible interpretation of the results obtained is as follows. In the absence of U-processes, only longitudinal phonons scatter from electrons in a pure conductor. In processes of "pure" phonon-electron scattering the transferred momentum is $\sim q$, the region of the interaction is $\sim 1/q$, and the interaction time is $\sim 1/qv_{\mathrm{F}}$. In an impure conductor, under condition $ql < 1$, the electron diffuses slowly in the interaction region. Therefore, the interaction time increases up to $\sim 1/Dq^2$ (D is the diffusion coefficient), and the process of pure phonon-electron scattering enhances by a factor $1/ql$, thus $1/\tau_{\text{ph-e}} \sim u^2/D$. Electron scattering from vibrating boundaries and defects generates another channel of phonon-electron scattering. In these processes the transferred electron momentum is $\sim p_{\mathrm{F}}$, and the corresponding phonon-electron scattering rate is also of the order of $\sim u^2/D$ due to large phase space for scattered states. If impurities and boundaries vibrate identically to the host atoms, the strong processes cancel each other. This cancellation corresponds to the fact that the deformation potential (or the phonon-electron vertex in the comoving frame [10, 11]) averaged over the Fermi surface is equal to zero. The interaction turns out to be by a factor $1/ql$ weaker than in the pure case, $1/\tau_{\text{ph-e}} \sim \omega_q^2 D/v_{\mathrm{F}}^2$. In other words, the effective phonon-electron coupling is $1/(ql)^2$ ($ql \ll 1$) times weaker than the coupling due to separate constituent processes discussed above. However, even a small amount of static scatterers results in an incomplete cancellation of the strong processes (the effective interaction is only by l/L factor weaker than the electron scattering from vibrating potential or disorder-enhanced pure phonon-electron interaction). Boundaries of conducting micro and nanostructures and rigid materials characterized by large acoustic impedance (diamond, Si_3N_4, SiO_2) are often described by the clamped-surface boundary condition [13], *i.e.*, zero displacement at the boundary. According to our results, such boundaries should drastically change the phonon-electron scattering in micro and nanostructures.

Vibrations of substitutional atoms result in the effect analogous to the effect considered here for static scatterers. We consider phonon modes with eigenfrequencies in the acoustic band of the host crystal. Rearrangement of the phonon states and change in the amplitude of vibrating atoms are given by the phonon Green function [14]. Relative amplitude of vibrations

of defects may be presented as $1 + \delta$, where δ depends on the mass and bound mismatches as well as on the phonon frequency (it goes to zero for long-wave phonons). If the mass of defects is 2-3 times larger or smaller than the mass of host atoms, the parameter δ is $\sim 5 \cdot 10^{-3}$ at $\omega_q \sim 0.01\omega_{\mathrm{D}}$ (ω_{D} is the Debye frequency) [14]. In the frame of our model, the effect of substitutional atoms may be evaluated by L, which is $\sim l/\delta$. For disordered metals with $l \sim 0.5$ nm, the corresponding value of L is $\sim 0.1\,\mu$m, and according to our calculations (see figs. 3 and 4), the effective phonon-electron coupling should significantly increase due to disorder. In our opinion, this effect has been observed in AuPd, TiAl disordered films at low temperatures [15]. The measured exponent, n, in the temperature dependence of the heat flux ($Q \propto \theta^n - T^n$, see eq. (27)) in metallic nanostructures has been found to be smaller than 5 [16] in agreement with our conclusions.

In summary, we calculate the phonon-electron relaxation rate (eqs. (21) and (23)) and the heat flux from hot electrons to phonons (eq. (27)) in a disordered conductor with the vibrating scattering potential and quasistatic scattering potential, which, for example, may be associated with rigid boundaries of micro and nanostructures. Contrary to the case of complete drag of electron scatterers by lattice, the presence of the quasistatic potential leads to enhancement of effective phonon-electron coupling. The relaxation rate of low-energy phonons enhances by a factor $(q^2 l L)^{-1}$ compared with the Pippard result.

* * *

This work is supported by the US ARO.

REFERENCES

[1] Peierls R., *Z. Phys.*, **88** (1934) 786.
[2] Pippard A. B., *Philos. Mag.*, **46** (1955) 1104.
[3] Ziman J. M., *Electrons and Phonons* (Clarendon, Oxford) 1960, p. 213.
[4] Kittel C., *Quantum Theory of Solids* (John Wiley & Sons, New York, London) 1963, p. 326.
[5] Kaveh M. and Wither N., *Phys. Rev B*, **36** (1987) 6339.
[6] Grünvald G. and Scharnberg K., *Z. Phys.*, **268** (1974) 197.
[7] Strictly speaking, this approach is not correct, if $\omega_q \leq Dq^2$. In the general case one should start with bare (unscreened) vertices and take into account peculiarities of the electron dielectric function. However, detailed calculations show that our final results for the phonon relaxation rate are valid also for phonons with $\omega_q \leq Dq^2$.
[8] Reizer M. Yu. and Sergeev A. V., *Zh. Eksp. Teor. Fiz.*, **92** (1987) 2291 (*Sov. Phys. JETP*, **65** (1987) 1291).
[9] Ptitsina N. G., Chulkova G. M., Il'in K. S. *et al.*, *Phys. Rev. B*, **56** (1997) 10089; Il'in K. S., Ptitsina N. G., Sergeev A. V. *et al.*, *Phys. Rev. B*, **57** (1998) 15623.
[10] Reizer M. Yu. and Sergeev A. V., *Zh. Eksp. Teor. Fiz.*, **90** (1986) 1056 (*Sov. Phys. JETP*, **63** (1986) 616).
[11] Rammer J. and Schmid A., *Phys. Rev. B*, **34** (1986) 1352.
[12] Kaganov M. I. and Peschanskii V. G., *Zh. Eksp. Teor. Fiz.*, **33** (1957) 1261 (*Sov. Phys. JETP*, **70** (1958) 970).
[13] Yu SeGi, Kim K. W., Stroscio M. A., Iafrate G. J. and Ballato A., *Phys. Rev. B*, **50** (1994) 1733; *Phys. Rev. B*, **51** (1994) 4695; Pipa V. I., Vasko F. T. and Mitin V. V., *J. Appl. Phys.*, **85** (1999) 2754.
[14] Bottger H., *Principles of the Theory of Lattice Dynamics* (Physic-Verlag, Berlin) 1983; Dawber P. G. and Elliott R. J., *Proc. R. Soc.*, **273** (1963) 222.
[15] Lin J. J. *et al.*, *Europhys. Lett.*, **29** (1995) 141 ; Wu C. Y. and Lin J. J., *Phys. Rev. B*, **50** (1994) 385; Wu C. Y. *et al.*, *Phys. Rev. B*, **57** (1998) 11232; Lin J. J., *Physica B*, **279** (2000) 191.
[16] Kauppinen J. P. and Pekola J. P., *Phys. Rev. B*, **54** (1996) R8353.